Star Formation Newsletter
No. 347 24-29

高橋実道（NAOJ）

24 Star Formation Regulation and Self-Pollution by Stellar Wind Feedback

25 ATOMS: ALMA Three-millimeter Observations of Massive Star-forming regions – V. Hierarchical fragmentation and gas dynamics in IRDC G034.43+00.24

26 Magnetic fields in star formation: a complete compilation of all the DCF estimations

27 Chemical survey of Class I protostars with the IRAM-30m

28 Testing Models of Triggered Star Formation with Young Stellar Objects in Cepheus OB4

29 Star burst in W49N presumably induced by cloud-cloud collision

25. ATOMS: ALMA Three-millimeter Observations of Massive Star-forming regions – V. Hierarchical fragmentation and gas dynamics in IRDC G034.43+00.24

Hong-Li Liu, Anandmayee Tej, Tie Liu, Namitha Issac, Anindya Saha, Paul F. Goldsmith, Jun-Zhi Wang, Qizhou Zhang, Sheng-Li Qin, Ke Wang, Shanghuo Li, Archana Soam, Lokesh Dewangan, Chang Won Lee, Pak-Shing Li, Xun-Chuan Liu, Yong Zhang, Zhiyuan Ren, Mika Juvela, Leonardo Bronfman, Yue-Fang Wu, Ken'ichi Tatematsu, Xi Chen, Di Li, Amelia Stutz, Siju Zhang, L. Viktor Toth, Qiu-Yi Luo, Feng-Wei Xu, Jinzeng Li, Rong Liu, Jianwen Zhou, Chao Zhang, Mengyao Tang, Chao Zhang, Tapas Baug, E. Mannfors, Eswaraiah Chakali, Somnath Dutta

★ We present new 3-mm continuum and molecular lines observations from the ATOMS survey towards the massive protostellar clump, MM1, located in the filamentary infrared dark cloud (IRDC), G034.43+00.24 (G34). The lines observed are the tracers of either dense gas (e.g. HCO+/H13CO+ J = 1-0) or outflows (e.g. CS J = 2-1). The most complete picture to date of seven cores in MM1 is revealed by dust continuum emission. These cores are found to be gravitationally bound, with virial parameter, $\alpha_{vir} < 2$. At least four outflows are identified in MM1 with a total outflowing mass of $\sim 45 M_{\odot}$, and a total energy of $\sim 1 \times 10^{47}$ erg, typical of outflows from a B0-type star. Evidence of hierarchical fragmentation, where turbulence dominates over thermal pressure, is observed at both the cloud and the clump scales. This could be linked to the scale-dependent, dynamical mass inflow/accretion on clump and core scales. We therefore suggest that the G34 cloud could be undergoing a dynamical mass inflow/accretion process linked to the multiscale fragmentation, which leads to the sequential formation of fragments of the initial cloud, clumps, and ultimately dense cores, the sites of star formation.

大質量星形成

重元素の生成等、周囲に大きな影響を与える。

形成領域が遠く、光学的に厚いガスに覆われているなど、観測が困難。

大質量形成はcloud, clump, core の
multi-scale fragmentation で進む。
質量の決定にはCore スケールの降着だけでなく、
より大きなスケールでのinflow も重要

本研究の対象
Filamentary IRDC, G034.43+00.24(G34)
中のmassive clump MM1, MM2
距離 ~ 3.7kpc
0.2-0.5 pc, 数百Msun
Olometric luminosity
MM1: 2.4x10^4 Lsun (B0-type YSO)
MM2: 1.4x10^4 Lsun (ultra-compacr HII region)

観測結果

ALMA による3mm の観測　(ATOMS survey の一部)

Continuum: 1.9" x 2.1", 1rms=0.3mJy/beam

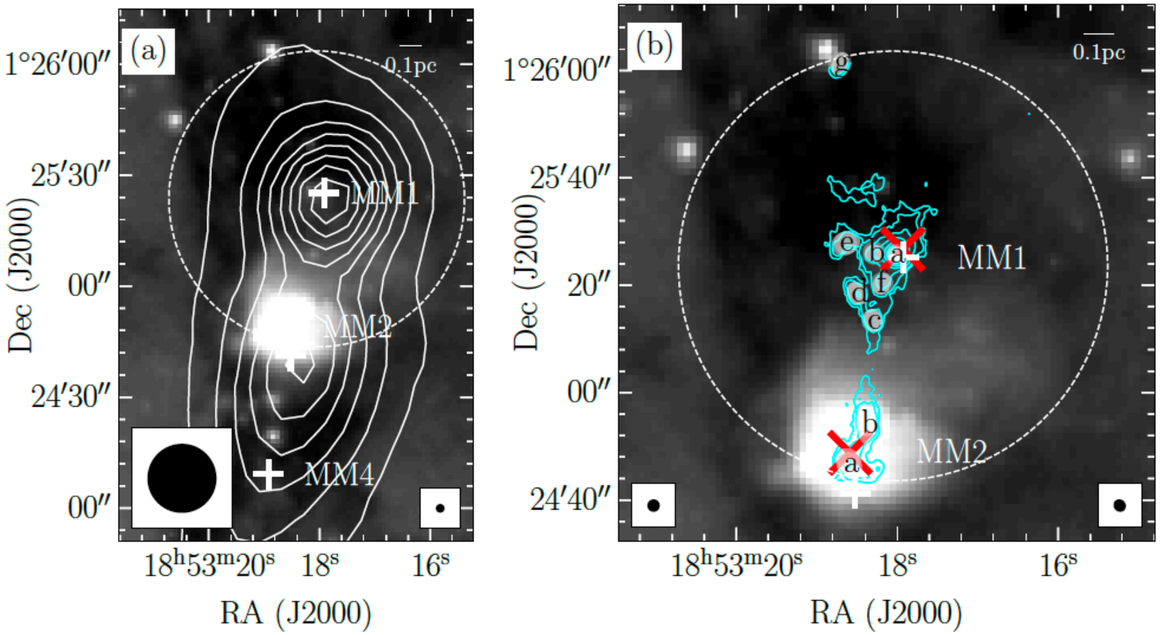

(a) Spitzer 8.0um image,
ATLASGAL 870um contours

(b) Spitzer 8.0um image,
ATOMS contours

ATOMS 視野が点線、MM2は半分しか含まれない

MM1で7個のcore を同定

コアの物理量

Name	RA (J2000)	Dec. (J2000)	$FWHM_{\rm dec}$ maj(″) × min(″)	PA deg	$F^{\rm int.}_{\rm 3mm}$ mJy	$F^{\rm P}_{\rm 3mm}$ mJy beam^{-1}	$R_{\rm core}$ 10^{-2} pc	$T_{\rm gas}$ K	$M_{\rm core}$ $M_\odot$	$\log(n_{\rm core})$ cm^{-3}	$\Sigma_{\rm core}$ g cm^{-2}	$V_{\rm lsr}$ km s^{-1}	ΔV km s^{-1}	$\alpha_{\rm vir}$
MM1-a	18:53:18.02	1:25:25.7	2.3 × 2.2	21.4	124.2 ± 0.8	54.7 ± 0.2	2.0 ± 0.2	100.0	199 ± 32	7.4	32.7	57.6 ± 0.2	4.5 ± 0.2	0.5
MM1-b	18:53:18.29	1:25:25.9	2.2 × 2.0	102.1	9.6 ± 0.1	9.6 ± 0.2	1.9 ± 0.2	27.6	58 ± 9	7.3	11.0	57.1 ± 0.2	2.9 ± 0.2	0.6
MM1-c	18:53:18.30	1:25:13.6	3.5 × 2.4	16.0	9.1 ± 1.0	2.8 ± 0.2	2.6 ± 0.2	14.2	115 ± 19	7.0	11.1	59.3 ± 0.2	1.1 ± 0.2	0.1
MM1-d	18:53:18.50	1:25:18.4	3.8 × 2.5	32.0	10.3 ± 1.0	3.0 ± 0.2	2.7 ± 0.2	13.8	136 ± 22	7.0	12.1	58.6 ± 0.2	1.8 ± 0.2	0.1
MM1-e	18:53:18.64	1:25:28.0	4.5 × 3.5	112.9	5.6 ± 0.1	1.9 ± 0.2	3.5 ± 0.3	22.6	42 ± 7	6.5	2.2	57.4 ± 0.2	1.6 ± 0.2	0.5
MM1-f	18:53:18.19	1:25:20.3	2.7 × 2.1	152.5	6.9 ± 0.1	5.5 ± 0.2	2.1 ± 0.2	18.6	65 ± 11	7.2	9.5	56.9 ± 0.2	3.3 ± 0.2	0.8
MM1-g	18:53:18.71	1:26:1.3	3.7 × 1.6	151.0	24.5 ± 0.9	9.1 ± 0.2	2.1 ± 0.2	21.7	196 ± 32	7.4	28.3	58.4 ± 0.2	3.4 ± 0.2	0.3
MM2-a	18:53:18.60	1:24:46.7	5.3 × 4.0	23.2	62.3 ± 1.5	9.8 ± 0.2	4.1 ± 0.3	100.0	97 ± 16	6.4	3.8	56.5 ± 0.2	2.5 ± 0.2	0.7
MM2-b	18:53:18.38	1:24:54.1	6.7 × 2.9	0.8	34.0 ± 1.4	5.5 ± 0.2	3.9 ± 0.3	20.8	281 ± 46	6.9	12.2	56.2 ± 0.2	2.7 ± 0.2	0.2

R_core ~ 0.02-0.04 pc, M_core ~ 42-281Msun

n_core ~ 0.2x10^7-2.8x10^7 cm^-3, Σ_core ~ 2-32 g/cm^2

Gravitationally bound

M_cl ~ 4.2x10^4 Msun ,n_cl ~ 2.6x10^5 cm^-3

cloud -> core のefficiency ~3%

H13CO+ (1-0)

optical depth 0.04-0.39

a: peak intensity. ダスト連続波より広がっている

b: moment 1 map. 速度勾配3-8 km/s/pc, Dは回転を示唆

c: line width. Cluster の中心で大きい

　star forming feadback, inflows

d: MM1で4つ、MM2で2つのoutflow

分子輝線

a-c: H13CO+ (1-0), d: CS(2-1)

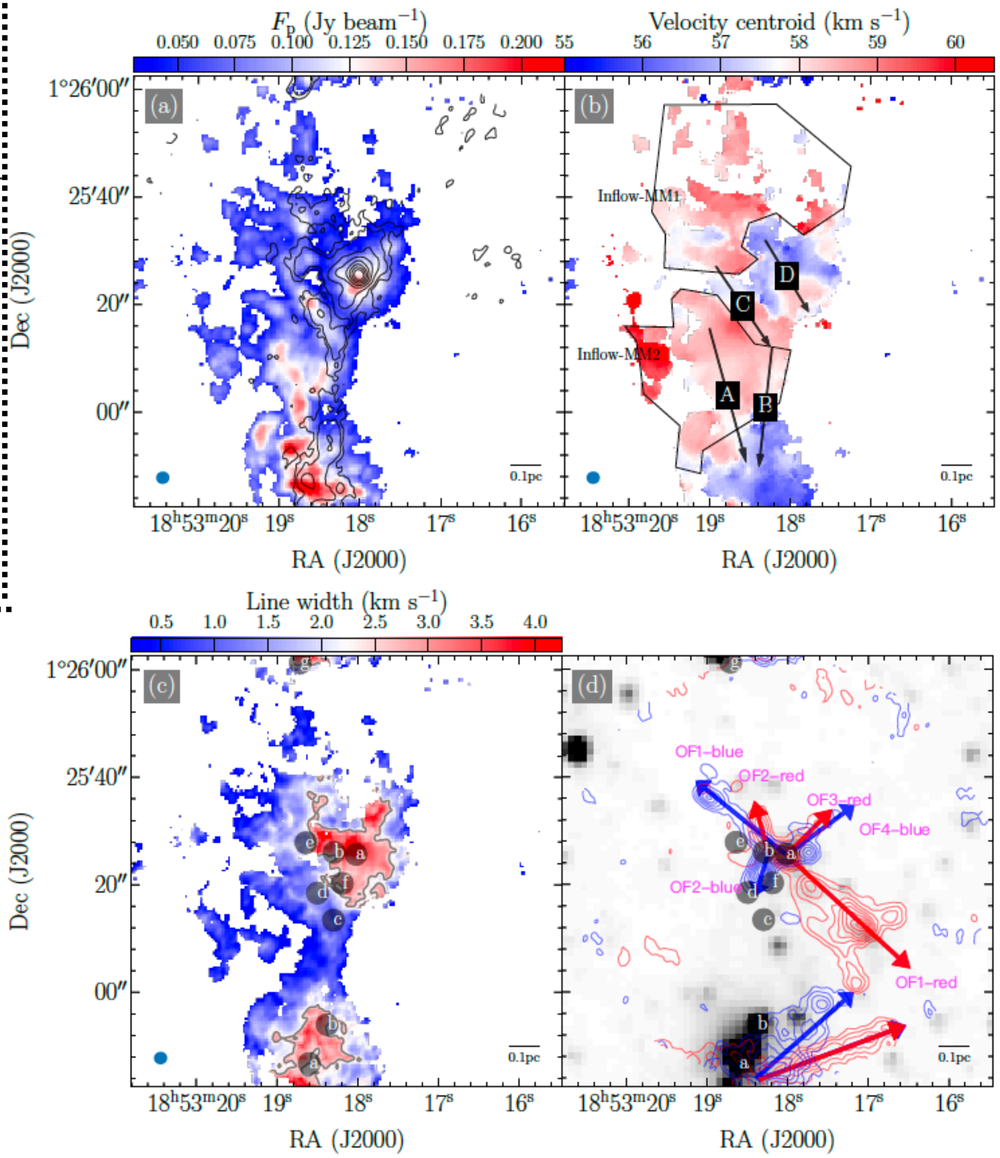

アウトフローの物理量

Table 2. CS (2-1) outflow parameters.

Outflow	Lobes	$< L >$ pc	$< V >$ km s^{-1}	$M_{\rm out}$ $M_\odot$	$P_{\rm out}$ $10^2 M_\odot$ km s^{-1}	$E_{\rm out}$ 10^{46}erg	$F_{\rm out}$ $10^{-3} M_\odot$ km s^{-1} yr^{-1}	$t_{\rm dyn}$ 10^3yr	$\dot{M}_{\rm acc}$ $10^{-5} M_\odot$ yr^{-1}
MM1-OF1	B+R	0.47 ± 0.07	14.6 ± 1.5	34.9 ± 1.7	5.1 ± 0.3	7.8 ± 0.4	16.2 ± 5.0	3.1 ± 0.8	$3.0 - 6.0$
MM1-OF2	B+R	0.18 ± 0.03	14.9 ± 1.5	8.0 ± 0.4	1.2 ± 0.1	1.8 ± 0.1	10.1 ± 3.3	1.2 ± 0.3	$2.0 - 4.0$
MM1-OF3	R	0.23 ± 0.02	18.2 ± 1.8	1.8 ± 0.1	0.3 ± 0.1	0.6 ± 0.1	2.6 ± 0.6	1.3 ± 0.2	$0.4 - 0.7$
MM1-OF4	B	0.14 ± 0.01	12.0 ± 1.2	1.1 ± 0.1	0.1 ± 0.1	0.2 ± 0.1	1.1 ± 0.3	1.2 ± 0.2	$0.2 - 0.3$
Total	–	–	–	44.7 ± 1.7	6.6 ± 0.3	10.2 ± 0.4	29.0 ± 5.0	–	$5.4 - 10.7$

Dの速度勾配のp-v図

各線はKeplerian rotation curve

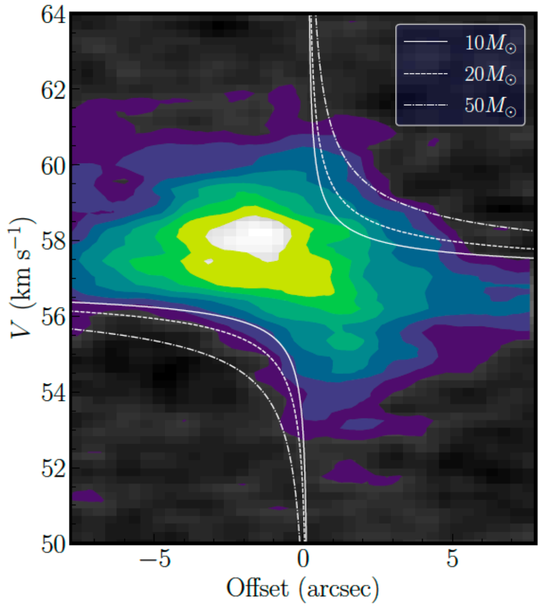

B0YSOだと思うと整合的

クランプ質量~200Msunとは一致しない

Jeans length, mass

Parameter	Cloud	Clump
$L^{\rm th}_{\rm Jeans}$ (pc):	~ 0.1	~ 0.06
$M^{\rm th}_{\rm Jeans}$ ($M_\odot$):	~ 2.6	~ 1.9
$L^{turb}_{\rm Jeans}$ (pc):	~ 0.4	~ 0.32
$M^{\rm turb}_{\rm Jeans}$ ($M_\odot$):	~ 180	~ 130
$L^{\rm ob}_{\rm frag}$ (pc):	~ 0.7	~ 0.12
$M^{\rm ob}_{\rm frag}$ ($M_\odot$):	~ 400–500	~ 115

乱流（H13CO+の速度分散）

まで考慮すると整合的

分子輝線の図(b)から、クランプへの

降着率を見積もる

-> ~3x10^-4Msun/yr >> $\dot{M}$acc

質量供給がスケールに依存する

シナリオを示唆

26. **Magnetic fields in star formation: a complete compilation of all the DCF estimations**

Junhao Liu, Keping Qiu, Qizhou Zhang ★

The Davis-Chandrasekhar-Fermi (DCF) method provides an indirect way to estimate the magnetic field strength from statistics of magnetic field orientations. We compile all the previous DCF estimations from polarized dust emission observations and re-calculate the magnetic field strength of the selected samples with the new DCF correction factors in Liu et al. (2021). We find the magnetic field scales with the volume density as $B \propto n^{0.57}$. However, the estimated power-law index of the observed $B - n$ relation has large uncertainties and may not be comparable to the $B - n$ relation of theoretical models. A clear trend of decreasing magnetic viral parameter (i.e., increasing mass-to-flux ratio in units of critical value) with increasing column density is found in the sample, which suggests the magnetic field dominates the gravity at lower densities but cannot compete with the gravity at higher densities. This finding also indicates that the magnetic flux is dissipated at higher column densities due to ambipolar diffusion or magnetic recennection, and the accumulation of mass at higher densities may be by mass flows along the magnetic field lines. Both sub-Alfvénic and super-Alfvénic states are found in the sample, with the average state being approximately trans-Alfvénic.

星間磁場

Zeeman 効果などで直接調べられる
B∝n^2/3 at n_H2>150 cm^-3
上限しか得られない場合がある。
より多いサンプルで統計を取りたい。

Davis-Chandrasekhar-Fermiで、
これまでのデータをすべて合わせて統計を取る。

Davis-Chandrasekhar-Fermi

Velocity dispersion と磁場のゆらぎから
磁束密度を得る

$$B_{\rm pos}^{\rm u,DCF53} \sim \sqrt{\mu_0 \rho} \frac{\delta v_{\rm los}}{\delta \phi},$$

速度、磁束のゆらぎが
Alfven波で説明できるときに正しい。

シミュレーションからcorrection factor が
得られている。~0.5程度

本研究ではLiu et al. 2021で得られた
correction factor を使って再計算する。

$$B_{\rm pos}^{\rm u,DCF53,est} \sim 0.28 \sqrt{\mu_0 \rho} \frac{\delta v_{\rm los}}{\delta \phi},$$ 一様成分

$$B_{\rm pos}^{\rm tot,DCF53,est} \sim 0.62 \sqrt{\mu_0 \rho} \frac{\delta v_{\rm los}}{\delta \phi},$$ 乱流込み

元データと本研究での値の比較

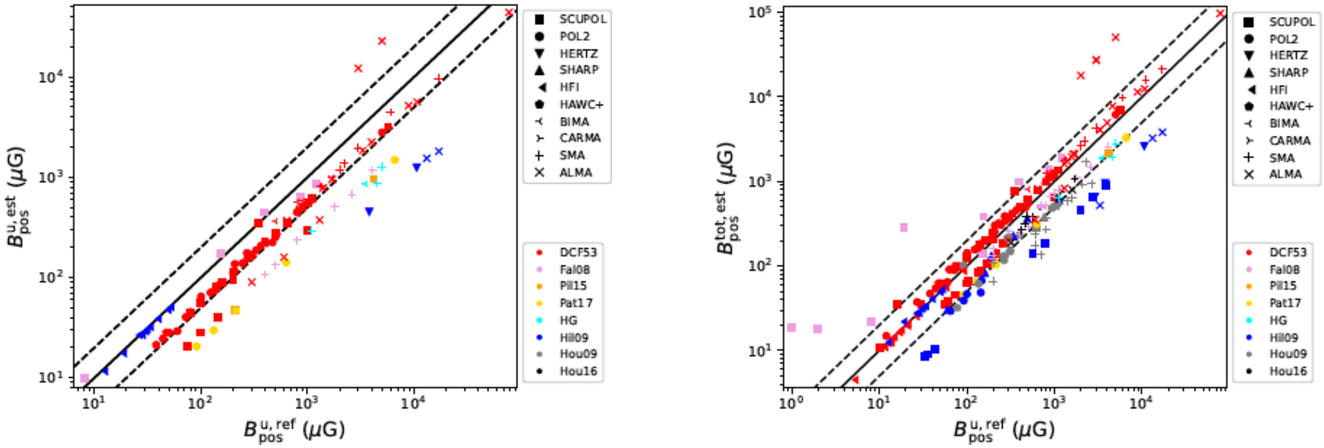

先行研究ではcorrection factor 0.5がよく使われるので、
基本的にそれとの違いが見える。

（他の要因は密度の評価など？）

B-n relation

B∝n^j とする。
理論的には、磁場が弱いときは j=2/3
磁場が強く、ambipolar diffusion 等がガスの収縮を決めるとき j<0.5

過去の文献値、一様成分　Zeemanの結果　本研究での再計算、乱流込み

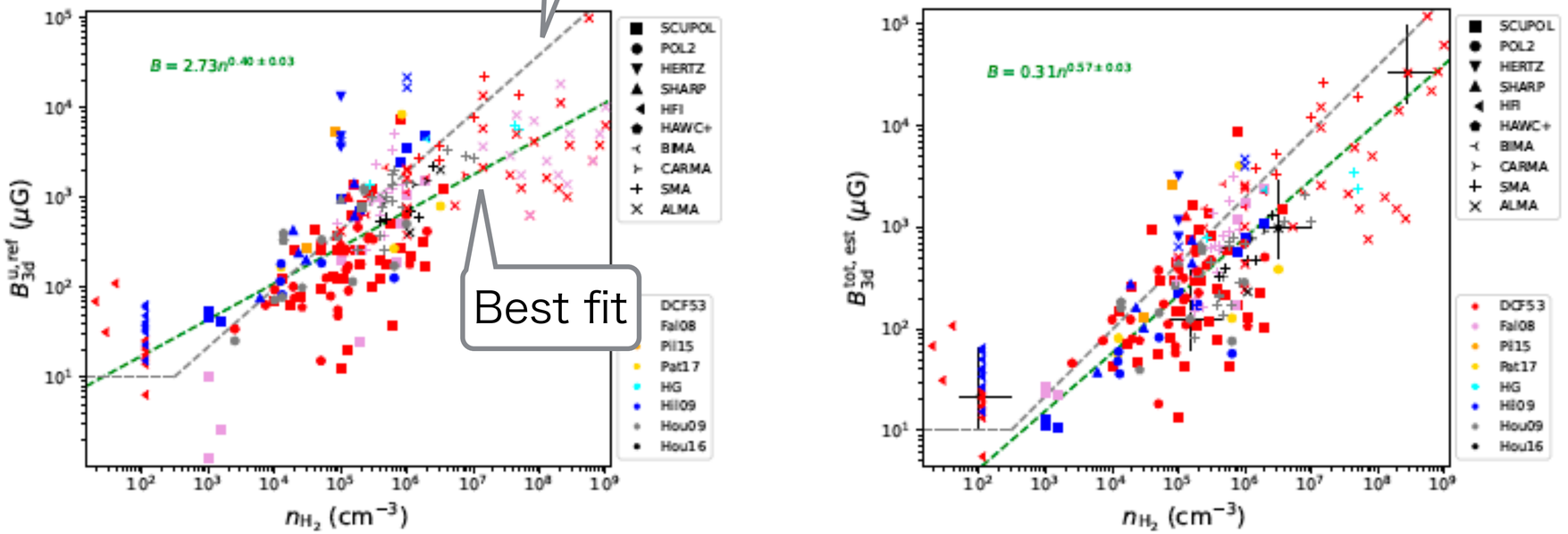

再計算した値のほうがばらつきは抑えられる。j=0.57
理論から予測される2つのベキの間の値。
Zeemanで得られた値より小さいが、不定性を考えると整合的。

DCFの問題点

$$\delta v_{\rm los}(B_{\rm t}/B)^{-1} \propto n^{\frac{j'}{2}}$$

として、観測からj'を得ると

$$B \propto n^{0.5+j'}$$

とかける。

右辺の密度は7桁程度変化
一方、左辺の各物理量は
1桁程度しか変わらない。
=> j~0.5の値になりやすい

B-N relation

自己重力に対してsuper-critical/sub-critical?

規格化したmass-to-flux ratio

$$\lambda_{\rm B} = \frac{1}{\alpha_{\rm B}} = \frac{M}{M_{\rm B}} = \mu_{\rm H_2} m_{\rm H} \sqrt{\frac{3\mu_0 \pi G}{2k}} \frac{N_{\rm H_2}}{B}$$

$$(k = (5-2i)/(3-i)\ ,\ n \propto r^{i})$$

本研究での再計算、乱流込み

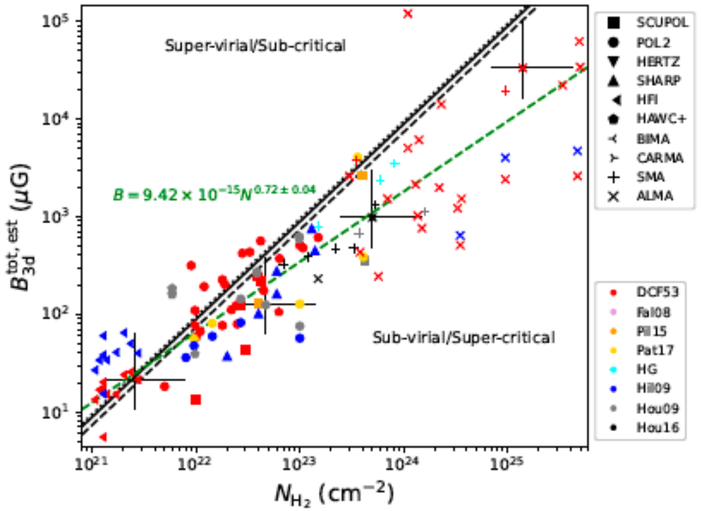

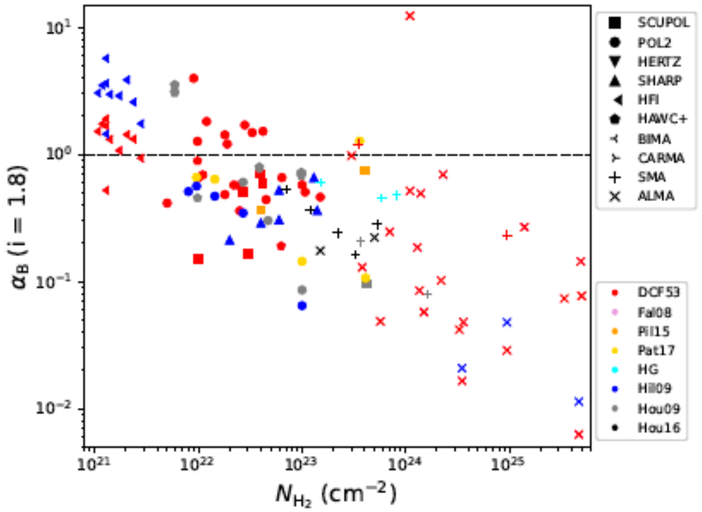

黒線がλ=1, 緑線がbest fit

低密度側でsub-critical, 高密度側でsuper-critical

Trans-critical point N_H2~3.4x10^21cm^-2, B~30uG

乱流速度

今回のサンプルにはSuper-Alfvenic, Sub-Alfvenic両方含まれる。

低密度、高密度側はSuper-Alfvenic

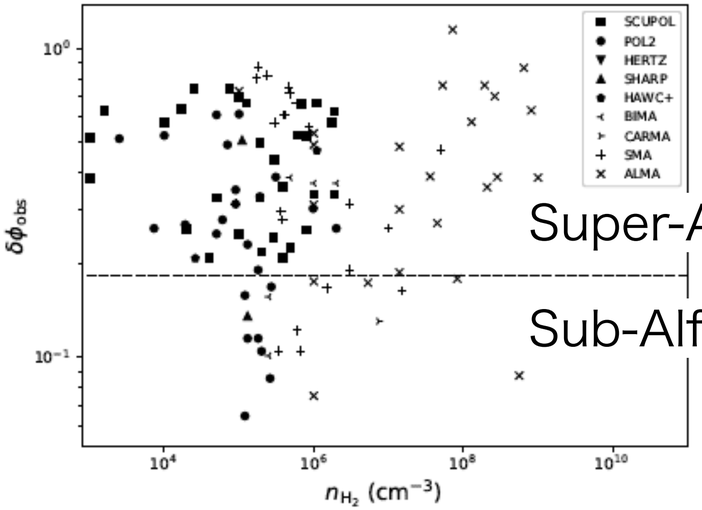

Super-Alfvenic

Sub-Alfvenic

(Correction factor の違いを見ているだけ？)

24. **Star Formation Regulation and Self-Pollution by Stellar Wind Feedback**

Lachlan Lancaster, Eve C. Ostriker, Jeong-Gyu Kim, Chang-Goo Kim ★
Stellar winds contain enough energy to easily disrupt the parent cloud surrounding a nascent star cluster, and for this reason have been considered candidates for regulating star formation. However, direct observations suggest most wind power is lost, and Lancaster21a,b recently proposed that this is due to efficient mixing and cooling processes. Here, we simulate star formation with wind feedback in turbulent, self-gravitating clouds, extending our previous work. Our simulations cover clouds with initial surface density $10^2 - 10^4\ M_\odot\,\mathrm{pc}^{-2}$, and show that star formation and residual gas dispersal is complete within 2 - 8 initial cloud free-fall times. The "Efficiently Cooled" model for stellar wind bubble evolution predicts enough energy is lost for the bubbles to become momentum-driven, we find this is satisfied in our simulations. We also find that wind energy losses from turbulent, radiative mixing layers dominate losses by "cloud leakage" over the timescales relevant for star formation. We show that the net star formation efficiency (SFE) in our simulations can be explained by theories that apply wind momentum to disperse cloud gas, allowing for highly inhomogeneous internal cloud structure. For very dense clouds, the SFE is similar to those observed in extreme star-forming environments. Finally, we find that, while self-pollution by wind material is insignificant in cloud conditions with moderate density (only $\lesssim 10^{-4}$ of the stellar mass originated in winds), our simulations with conditions more typical of a super star cluster have star particles that form with as much as 1% of their mass in wind material.

27. Chemical survey of Class I protostars with the IRAM-30m

S. Mercimek, C. Codella, L. Podio, E. Bianchi, L. Chahine, M. Bouvier, A. Lopez-Sepulcre, R. Neri, C. Ceccarelli ★

Class I protostars are a bridge between Class 0 protostars, and Class II protoplanetary disks. Recent studies show gaps and rings in the dust distribution of disks younger than 1 Myr, suggesting that planet formation may start already at the Class I stage. To understand what chemistry planets will inherit, it is crucial to characterize the chemistry of Class I sources and to investigate how chemical complexity evolves from Class 0 protostars to protoplanetary disks. The goal is twofold: to obtain a census of the molecular complexity in a sample of four Class I protostars, and to compare it with the chemical compositions of earlier and later phases of the Sun-like star formation process. We performed IRAM-30m observations towards Class I objects (L1489-IRS, B5-IRS1, L1455-IRS1, and L1551-IRS5). The column densities of the detected species are derived assuming LTE or LVG. We detected 27 species: C-chains, N-bearing, S-bearing, Si-bearing species, deuterated molecules, and iCOMs. Different spectral profiles are observed: narrow lines towards all the sources, broader lines towards L1551-IRS5, and line wings due to outflows. Narrow c-C3H2 emission originates from the envelope. The iCOMs in L1551-IRS5 reveal the occurrence of hot corino chemistry, with CH3OH and CH3CN lines originating from a compact and warm region. Finally, OCS and H2S seem to probe the circumbinary disks in the L1455-IRS1 and L1551-IRS5 binary systems. The deuteration in terms of elemental D/H in the molecular envelopes and hot corino are derived. In addition, B5 IRS1, L1455-IRS1 and L1551-IRS5 show a low excitation methanol line, suggesting an origin from an extended structure, plausibly UV illuminated. The abundance ratios of iCOMs with respect CH3OH measured towards the L1551-IRS5 hot corino and the deuteration in our sample are comparable to that estimated at earlier stages, as well as to that found in comets.

28. Testing Models of Triggered Star Formation with Young Stellar Objects in Cepheus OB4

Abby Mintz, Joseph L. Hora, Elaine Winston ★ OB associations are home to newly formed massive stars, whose turbulent winds and ionizing flux create H II regions rich with star formation. Studying the distribution and abundance of young stellar objects (YSOs) in these ionized bubbles can provide essential insight into the physical processes that shape their formation, allowing us to test competing models of star formation. In this work, we examined one such OB association, Cepheus OB4 (Cep OB4) - a well-suited region for studying YSOs due to its Galactic location, proximity, and geometry. We created a photometric catalog from Spitzer/IRAC mosaics in bands 1 (3.6 μm) and 2 (4.5 μm). We supplemented the catalog with photometry from WISE, 2MASS, IRAC bands 3 (5.8 μm) and 4 (8.0 μm), MIPS 24 μm, and MMIRS near IR data. We used color-color selections to identify 821 YSOs, which we classified using the IR slope of the YSOs' spectral energy distributions (SEDs), finding 67 Class I, 103 flat spectrum, 569 Class II, and 82 Class III YSOs. We conducted a clustering analysis of the Cep OB4 YSOs and fit their SEDs. We found many young Class I objects distributed in the surrounding shell and pillars as well as a relative age gradient of unclustered sources, with YSOs generally decreasing in age with distance from the central cluster. Both of these results indicate that the expansion of the H II region may have triggered star formation in Cep OB4.

29. Star burst in W49N presumably induced by cloud-cloud collision

Ryosuke Miyawaki, Masahiko Hayashi, Tetsuo Hasegawa ★ We present high resolution observations of CS(J=1-0), H13CO+ (J=1-0), and SiO(v=0:J=1-0) lines, together with the 49GHz and 86GHz continuum emissions, toward W49N carried out with Nobeyama Millimeter Array. We identified 11 CS, 8 H13CO+, and 6 SiO clumps with radii of 0.1-0.5pc. The CS and H13CO+ clumps are mainly divided into two velocity components, one at 4kms-1 and the other at 12kms-1, while the SiO clumps have velocities between the two components. The SiO emission is distributed toward the UCHII ring, where the 4kms-1 component clumps of CS and H13CO+ also exist. The 12kms-1 component clumps of CS are detected at the east and west of the UCHII ring with an apparent hole toward the ring. The clump masses vary from $4.4\text{x}10^2$ $M_\odot$ to $4.9\text{x}10^4$ $M_\odot$ with the mean values of $0.94\text{x}10^4$ $M_\odot$, $0.88\text{x}10^4$ $M_\odot$, and $2.2\text{x}10^4$ $M_\odot$ for the CS, H13CO+, and SiO clumps, respectively. The total masses derived from CS, H13CO+, and SiO clumps are $1.0\text{x}10^5$ $M_\odot$, $0.70\text{x}10^5$ $M_\odot$, and $1.3\text{x}10^5$ $M_\odot$, respectively, which agree well with the corresponding virial masses of $0.71\text{x}10^5$ $M_\odot$, $1.3\text{x}10^5$ $M_\odot$, and $0.88\text{x}10^5$ $M_\odot$, respectively. The average molecular hydrogen densities of the clumps are $0.90\text{x}10^6$ cm-3, $1.4\text{x}10^6$ cm-3, and $7.6\text{x}10^6$ cm-3 for the CS, H13CO+ and SiO clumps, respectively. The density derived from the SiO clumps seems significantly higher than those from the others, probably because the SiO emission is produced in high density shocked regions. The free fall time scale of the clumps is estimated to be $3\text{x}10^4$ yr, which gives an accretion rate of $3\text{x}10-3-1$ $M_\odot$ /yr onto a stellar core. The observed clumps are, if they are undergoing free fall, capable of producing dozens of massive stars in the next 10^5 yr. We propose a view that pre-existing two clouds collided with each other almost face-on to produce the observed clumps and triggered the burst of massive star formation in W49N.